Important role of projectile excitation in ^{16}O + ^{60}Ni and ^{16}O + ^{27}Al scattering at intermediate energies

V. A. B. Zagatto,[1,*] F. Cappuzzello,[2,3] J. Lubian,[1] M. Cavallaro,[2] R. Linares,[1] D. Carbone,[2] C. Agodi,[2] A. Foti,[2] S. Tudisco,[2] J. S. Wang,[4] J. R. B. Oliveira,[5] and M. S. Hussein[5,6,7]

[1]*Instituto de Física da Universidade Federal Fluminense, 24210-346, Niterói, Rio de Janeiro, Brazil*
[2]*Istituti Nazionali di Fisica Nucleare, Laboratori Nazionali del Sud, 95123, Catania, CT, Italy*
[3]*Dipartimento di Fisica e Astronomia Università di Catania, I-95123, Catania, CT, Italy*
[4]*Institute of Modern Physics, Chinese Academy of Sciences, Lanzhou, 730000, China*
[5]*Instituto de Física da Universidade de São Paulo, 05508-090, São Paulo, São Paulo, Brazil*
[6]*Instituto Tecnólogico de Aeronáutica, Departamento de Ciência e Tecnologia Aeroespacial, 12.228-900 São José dos Campos, São Paulo, Brazil*
[7]*Instituto de Estudos Avançados, Universidade de São Paulo, 05508-970 São Paulo, São Paulo, Brazil*

The elastic scattering angular distribution of the ^{16}O + ^{60}Ni system at 260 MeV was measured in the range of the Rutherford cross section down to seven orders of magnitude. The cross sections of the lowest 2^+ and 3^- inelastic states of the target were also measured over several orders of magnitude. Coupled-channel (CC) calculations were performed and are shown to be compatible with the whole set of data only when including the excitation of the projectile and when the deformations of the imaginary part of the nuclear optical potential are taken into account. Similar results were obtained when the procedure is applied to the existing data on ^{16}O + ^{27}Al elastic and inelastic scattering at 100 and 280 MeV. An analysis in terms of dynamical polarization potentials (DPP) indicates the major role of coupled-channel effects in the overlapping surface region of the colliding nuclei.

I. INTRODUCTION

Elastic scattering is usually the simplest and most intense channel in nuclear collisions. Notwithstanding, studies are commonly performed that aim to investigate the nucleus-nucleus potential or the effect of nonelastic channels. There are many examples in the literature where a detailed description of elastic scattering is essential to understand emerging phenomena, like the threshold anomaly on tightly [1–3] and weakly [4–7] bound nuclei, breakup dynamics [8–11], and the nuclear rainbow [12–15].

Most of the above-mentioned studies are performed at energies around the Coulomb barrier, where the number of open channels is relatively small. Even in this region, coupled-channel calculations including all the open channels are challenging, as demonstrated in Refs. [16–20]. At higher incident energies, they become even more difficult as more channels are energetically open.

Recent advances in experimental techniques allow the measurement of high-precision and accurate data down to very low absolute cross sections (∼nb/sr). The increased resolution reveals new phenomena [21,22] and provides information on channel couplings that could not be studied in detail before [23,24]. From the theoretical side, the main challenge is to incorporate, in a simple and accurate model, the complex picture arising from the full many-body scattering problem. In

particular, a reaction model that uses a global potential (which captures the average features of the scattering) and requires few relevant reaction channels is highly desirable.

In Refs. [25] and [26], direct reaction calculations using global potentials have already been performed, coupling only a few relevant reaction channels. The first work demonstrated that the 3^- state of the ^{16}O nucleus is crucial for the appearance of a secondary rainbow structure in the elastic scattering of ^{16}O + ^{12}C reaction at 330 MeV. The effect of couplings to ^{16}O states was not fully explored in the analysis of the ^{16}O + ^{27}Al system (at 280 MeV) in Ref. [26]. Studying the possible effect of projectile excitation on a third system would help to elucidate this question. In the present work, we carefully investigate one more reaction, ^{16}O + ^{60}Ni at $E = 260$ MeV, to better understand the role of the excitation of the projectile. We chose this system because high-precision experimental data are available on both the elastic and inelastic scatterings.

In the next section, some details of the experiment are presented. The theoretical analysis is presented in Sec. III. In Sec. IV, discussions about the normalization of the imaginary potentials and the coupling effects of each channel on the effective potential are made. Finally, in the last section the conclusions are presented.

II. EXPERIMENTAL DETAILS

The experimental data have been measured at the MAGNEX large acceptance spectrometer [27,28] at INFN-LNS (Catania, Italy). The ^{16}O^{8+} beam impinged on isotopically
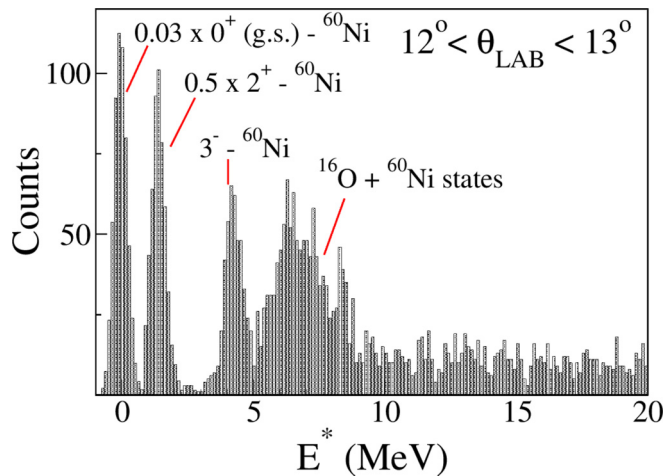
*vinicius.zagatto@gmail.com

FIG. 1. Energy spectrum for the ^{16}O + ^{60}Ni reaction at 260 MeV between 12° and 13° (laboratory framework). The most relevant peaks are identified in the figure. Note that peaks corresponding to the elastic and first inelastic states are scaled for better visualization.

enriched ^{60}Ni targets. A 150 μg/cm^2 thick target was used for measurements at forward angles ($5° < \theta_{LAB} < 15°$), and a 500 μg/cm^2 thick one was used for the large angular region ($8° < \theta_{LAB} < 45°$). The scattered ejectiles were momentum selected by the spectrometer and the trajectory parameters (i.e., position, incident angles, energies) were measured by the focal plane detector (FPD) [29]. Particle identification and high-order trajectory reconstruction techniques allowed us to recover the scattered energies and angles at the target position [30,31]. Details of ^{16}O + ^{27}Al data reduction can be found in Refs. [32,33].

A typical energy spectrum of the ^{16}O + ^{60}Ni reaction is presented in Fig. 1. The energy resolution is about 600 keV. The 0^+ ground state and the 2^+ ($E^* = 1.33$ MeV) and 3^- ($E^* = 4.04$ MeV) excited states of target were clearly resolved from each other. It is also noticed the presence of a large structure in

the 5- to 9-MeV region, composed by several states. The same structure appears in ^{60}Ni(α,α') scattering data of Ref. [34]. In this energy range, numerous excited states of projectile [$0(2)^+$, 3^-, 2^+, 1^-, 2^-] and target are expected to be populated.

The angular distributions of the absolute elastic and inelastic cross sections were extracted from measured yields down to a remarkable value of 10^{-7} σ_{Ruth} and are shown in Fig. 2. A systematic error in the cross section is common to all data points and it is not included in the error bars. This kind of error comes from two sources: the determination of the target thickness (obtained previously measuring the energy loss of α particles) and the beam integration by the Faraday cup (small noise induced in the Faraday cup cabling). The uncertainties represented in Fig. 2 come from other sources, such as the solid angle determination (correlated to the error in the measurement of the central angular position of MAGNEX spectrometer) and the statistical error (greater at backward angles). No background subtraction was performed. A possible contribution from contaminants in the ^{60}Ni target (usually from carbon or oxygen buildup during beam exposure) is negligible. At very forward angles ($\theta_{c.m.} < 7.5°$), the first inelastic state of ^{60}Ni slightly interferes with the elastic peak due to the low resolution of the detector at this angular region. See the Supplemental Material [35] for tables of the scattering data. For further information about the uncertainty propagation, one may consult Ref. [31].

The large uncertainty in the measured elastic data in the region of $\theta_{c.m.} > 30°$ do not allow us to define a fine oscillatory pattern of scattering as done previously for the ^{16}O + ^{27}Al reaction at 280 MeV [26] due to the low number of counts in each angle.

III. THEORETICAL FRAMEWORK

As stated before, at low energies only a few reaction mechanisms are important and are usually included in the coupling scheme of CC calculations. Thus, the only imaginary potential needed is a internal potential to the barrier that accounts for
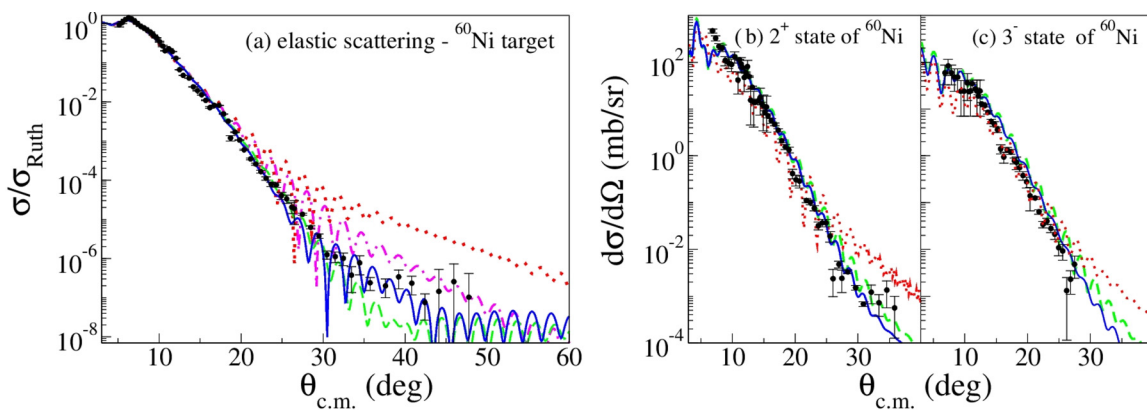

FIG. 2. Angular distributions of ^{16}O + ^{60}Ni: (a) Elastic scattering showing different calculations. The dot-dashed magenta line shows the optical model calculation with nuclear São Paulo potential. The dashed green line shows the CC calculations including the first 2^+ and 3^- inelastic states of target. The solid blue line shows the results of CC calculation including the target excitation and also the first inelastic state of projectile. The dotted red line shows the calculations including all the mentioned couplings but disregarding the deformation of the imaginary potential. (b) 2^+ inelastic distribution of target. The calculations follow the same color representation and curves as in panel (a). (c) 3^- inelastic distribution of target. The calculations follow the same color representation and curves as in panel (a).

the loss of flux to fusion channel. When the energy increases, the number of direct reaction channels increases rapidly and it is almost impossible to couple all of them in CC calculations. This is especially true in the case of broad resonances (giant resonances) and high excited states, for which there is no spectroscopic information. Therefore, the CC calculation is performed using explicit coupling of the elastic channel to several inelastic channels corresponding to the excitation of collective states where spectroscopic information is available, and account for the coupling to the other high-energy collective channels implicitly through the use of a deformed complex coupling potential. Optical model and CC calculations were performed in order to analyze the data using the FRESCO code [36].

A. The ^{16}O + ^{60}Ni system

In the ^{16}O + ^{60}Ni calculations, the 2^+ and 3^- excited states of target were included in the coupling scheme. The 3^- ($E^* = 6.13$ MeV) excitation of projectile was also considered. The real nuclear potential used in the calculations was the double-folding São Paulo potential (SPP), V_{SPP} [37–39]. In Ref. [40], it was demonstrated that elastic scattering of several systems over a wide energy range is well described using "bare" (no couplings are considered) optical potential defined as

$$U_{bare} = (1 + 0.8i)V_{SPP}. \tag{1}$$

The SPP potential is the nonlocal version of the double-folding interaction. The form used in the analysis of the data is the local, energy-dependent, equivalent potential; see Refs. [37–39]. The numerical factor 0.8 in the imaginary part of the bare potential above was fixed by adjusting a large set of data, which accounts for flux loss to other channels not explicitly included in the coupling scheme, as excited states and single-nucleon knockouts [41]. The results considering such systematics for ^{16}O + ^{60}Ni and ^{16}O + ^{27}Al reactions are, from now on, represented by a dot-dashed magenta line.

In Fig. 2, it is possible to notice that systematics gives a poor description of data for angles larger than $20°$. One should remember that this systematics was originally obtained for energies close to the Coulomb barrier, including data of cross sections (normalized by the Rutherford one) around 10^{-3} to 10^{-4}. A further improvement consisted in the coupling of the above-mentioned collective inelastic channels keeping the same bare potential. From now on, calculations considering the coupling of the inelastic channels of the target will be represented by a green dashed line. From calculations of ^{16}O + ^{27}Al reaction at 280 MeV reported in Ref. [26], it was noticed that the simple inclusion of inelastic channels was not sufficient to reproduce elastic scattering data at large angles. The coupling of α transfer channel (the one with most favored Q value) using realistic spectroscopic amplitudes did not modify the results. It was also discovered that the phase of the Fresnel oscillations in the theoretical results and the experimental data was not the same, clearly implying that additional reaction channels are required to be coupled in calculations in order to reproduce the full angular range covered by experimental data.

In Ref. [42], it is shown that the deformation of the imaginary part of the nuclear potential (when considering the coupling of the inelastic channels) can play an important role in the ^{182}W(d,d')^{182}W reaction. This result is in accordance with the Bohr-Mottelson unified model [43,44]. References [45,46] claimed that, even for light ions, the inclusion of the deformation of the imaginary part may provide evidence that there is a strong interference between the Coulomb and nuclear contributions, especially when collective excitations of the nuclei are present. Giant resonances (GR) can, in principle, act as important doorway states for nuclear scattering, since they represent small amplitude oscillations of nuclei. Very few collective degrees of freedom are involved in GR and consequently their overlap to the nuclear ground state can be large. However, not much is known about the effect of the GR on the elastic scattering. At the bombarding energies discussed here, high-lying states of nuclei can be accessed (including giant resonances), redistributing part of the flux from the low-lying excited states. A detailed description of the coupling to all GR would require several parameters, as multipolarities, centroids, and widths. Instead, in the present calculations, a different approach is proposed, by deforming of the imaginary part of the nuclear potential.

For deforming the imaginary part of the optical nuclear potential, the same prescription adopted for the deformation of its real part is adopted. This means that a multipole expansion of the optical potential is performed considering up to the octupole term. The radial part of the form factor are the derivatives of the potential. So, the transition operator is given by a polynomial expansion where each term is composed by the product of the deformation parameter, the radial derivative and the spherical function. Because of the large deformation parameter of the ^{16}O excited state, an option in the FRESCO code guarantees the volume conservation up to second-order correction.

For the ^{60}Ni nucleus, the excited states are described within the context of the vibrational model. In the calculations, the reduced transition probabilities $B(E2) \uparrow = 0.093$ e^2 b^2 for quadrupole state and $B(E3) \uparrow = 0.021$ e^2 b^3 for the octupole state, are those reported in Refs. [47] and [48], respectively. The $B(E3) \uparrow = 0.0015$ e^2 b^3 for the 3^- excited state of ^{16}O projectile was taken from Ref. [48]. Since this is the only state of the projectile coupled in the calculations, there is no difference when considering a vibrational or a rotational model for the excitation.

In all calculations, the finite diffuseness of nuclear surfaces (discussed in Ref. [49]) was considered. The respective δ deformation lengths and the reduced matrix elements used in the calculations were obtained from these experimental values using expressions reported in Ref. [36]. Calculations coupling the inelastic excitations of target and projectile are represented, from now on, by a solid blue line. Finally, calculations considering all the above-mentioned couplings but disregarding the deformation of imaginary part of nuclear potential will be presented as a red dotted line.

The inclusion of the 2^+ and 3^- inelastic states of the target ^{60}Ni in the CC calculations was not sufficient to reproduce the elastic scattering at large angles [Fig. 2(a)]. Several calculations were performed in an attempt to obtain a proper

imaginary normalization that reproduces data; however, this procedure did not improve the agreement between the experimental data and the theoretical elastic angular distributions (especially at large angles). The inclusion of the projectile excitation in the calculations (solid blue line), using the SPP optical potential, gives a remarkable good description of elastic scattering [Fig. 2(a)]. The calculation considering all the previous excitations and no deformation in the imaginary nuclear potential (red dotted line) does not describe the data properly, indicating the necessity of deforming the imaginary term.

Figures 2(b) and 2(c) show the inelastic angular distributions of ^{60}Ni 2^+ and 3^- states, respectively. CC calculations including the already-mentioned states (solid blue lines) show good agreement with data. Reference [50] shows that the 3^- state of ^{16}O can be interpreted as the isoscalar octupolar giant mode. The relevance of such state for a successful data analysis may indicate the importance of GR in elastic and quasielastic scattering.

We emphasize once again that the numerical factor 0.8 multiplying the imaginary part of the bare potential in our CC calculations accounts for the high energy of the explored reaction. As many channels are open at such energy, it is necessary to take into account the loss of flux to all processes that have not been explicitly considered. This effect is particularly important here since we are exploring the internal region of the reacting system where the flux dissipation effect is stronger.

B. The ^{16}O + ^{27}Al system

The same calculation approach can also describe the elastic and inelastic angular distributions measured in Ref. [26] for ^{16}O + ^{27}Al reaction at 280 MeV. In the ^{16}O + ^{27}Al spectrum (see Fig. 1 in Ref. [26]), it was possible to distinguish the elastic channel from a composition of five excited states of target: $1/2^+$ ($E^* = 0.84$ MeV), $3/2^+$ ($E^* = 1.01$ MeV), $7/2^+$ ($E^* = 2.21$ MeV), $5/2^+$ ($E^* = 2.73$ MeV), and $9/2^+$ ($E^* = 3.00$ MeV). The respective reduced transition probabilities $B(E2) \uparrow$ values are 0.004, 0.019, 0.004, 0.007, and 0.004 e^2 b^2. Again, a large structure at ~6 MeV containing excited states of the projectile and target has been observed. The $B(E2) \uparrow$ of ^{27}Al multiplet states have already been experimentally determined and can be found in Ref. [51]. Figures 3(a) and 3(b) show angular distributions for the ^{16}O + ^{27}Al elastic and inelastic scatterings, respectively.

We reiterate that the bare optical potential calculations and the CC calculations with the inclusion of the already-mentioned target excited states are not sufficient to describe data. The inclusion of the 3^- projectile excitation in the CC calculations is mandatory for a successful description of both elastic and inelastic scattering angular distributions. This suggests that taking into account the coupling to the 3^- state of the projectile ^{16}O is important at energies well above the barrier; however, further studies must be performed.

In particular, without the inclusion of the projectile excitation and the deformation of the imaginary part of optical potential, it was not possible to find the right phase of the oscillation pattern of elastic scattering [inset of Fig. 3(a)].
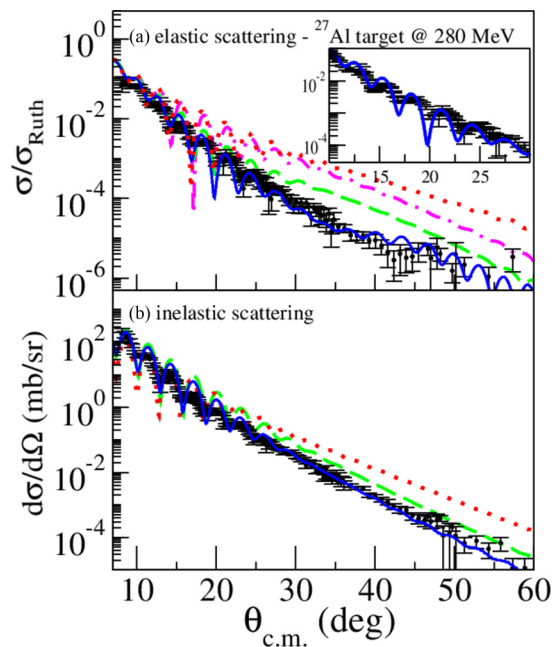

FIG. 3. Angular distributions of ^{16}O + ^{27}Al at 280 MeV: (a) Elastic scattering. The dot-dashed magenta line shows the optical model calculation with the nuclear São Paulo potential. The dashed green line shows the CC calculations including the inelastic states of the target (see text for details). The solid blue line shows the results of CC calculation including the target excitation and also the first inelastic state of projectile. The dotted red line shows the calculations including all the mentioned couplings but disregarding the deformation of the imaginary potential. (b) Inelastic states of target. The lines represent the summed total inelastic cross section. The calculations follow the same color representation and curves as in panel (a).

Without the deformation of the imaginary nuclear potential, the data are not well reproduced (red dotted line).

In Fig. 3(b), the experimental cross section is the sum of the quintuplet of inelastic channels. The ones that most contribute are the $1/2^+$ and $9/2^+$ (the latter at the largest angles). The experimental angular oscillations on the cross sections (as well as its absolute value) are well reproduced.

There are several differences in the present calculations with those performed in Ref. [26]. In the previous calculations, the excited states of ^{27}Al were treated as a hole in the 2^+ state of ^{28}Si. A poor description of elastic scattering was achieved in this framework (Fig. 3(a) of Ref. [26]). Also on those calculations, the proton and α transfer channels were considered; however, no satisfactory description of elastic channel was found (Fig. 3(c) of Ref. [26]). A good description (Fig. 4(a) of Ref. [26]) of data up to $\theta_{c.m.} = 40°$ was found when the normalization of the real part of nuclear potential was changed to a 0.6 factor; however, no explanation was found for it. Even on this previous work, it was said that a great effect due the resonant states could be the reason for the discrepancies between calculations and data. The main difference between that work and the present one is the deformation of the imaginary part of nuclear optical potential to take into account possible couplings to collective states
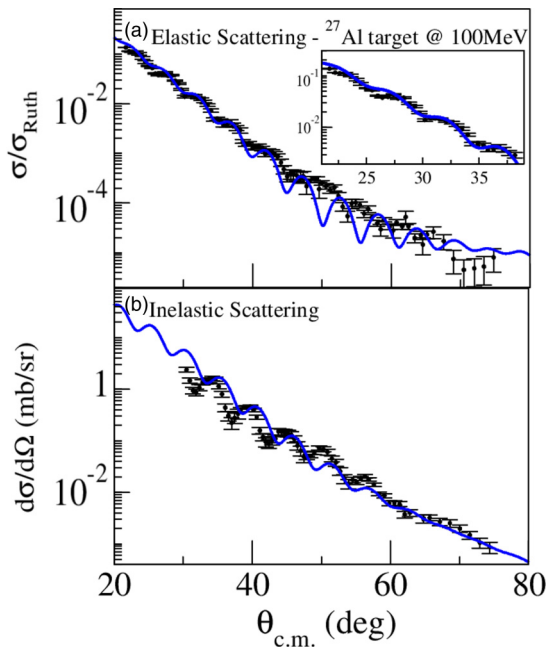
FIG. 4. Angular distributions of $^{16}\text{O} + ^{27}\text{Al}$ at 100 MeV: (a) Elastic scattering. The solid blue line shows the results of CC calculation including the target excitation and also the first inelastic state of projectile. (b) Inelastic states of target. The lines represent the summed total inelastic cross section.

not included explicitly, as the coupling of the 3^- state of the projectile, which also revealed to be extremely important in calculations. One must also observe that the present calculation describes the backward scattering data ($\theta_{\text{c.m.}} > 40°$) better than the previous one.

IV. DISCUSSION

In the calculations of $^{16}\text{O} + ^{27}\text{Al}$ reaction at 280 MeV, the $(1 + 0.8i)V_{\text{SPP}}$ nuclear potential was utilized (same imaginary normalization of 0.8 as that of the ^{60}Ni case). At lower energies, one expects that the numerical factor 0.8 to become smaller. This statement was tested by performing the same type of calculations for the $^{16}\text{O} + ^{27}\text{Al}$ reaction at 100 MeV, whose data are presented in Ref. [22]. The comparison of data from Ref. [22] and the present calculation is presented in Fig. 4.

For the lower energy, a good description of elastic [Fig. 4(a)] and inelastic [Fig. 4(b)] channels were obtained using a 0.45 normalization for the imaginary part. The decrease in normalization was expected since, at this energy, the number of open channels in the reaction is smaller when compared to the higher one. The comparison of the present calculation with the one presented in Ref. [22] demonstrates the importance of considering the coupling of projectile excitation and the deformation of imaginary potential, since they were not considered previously. In the previous work, it was not possible to reproduce the phase of oscillations in elastic scattering (inset of Fig. 2 of the previous work). This could be achieved in the present paper, as demonstrated in the inset of Fig. 4(a).

The present calculations also reproduced the data of the elastic scattering of $^{16}\text{O} + ^{60}\text{Ni}$ at 42-MeV incident beam

energy (from Ref. [52]), using an imaginary potential 40 times smaller (V_{bare} with 0.02 normalization of the imaginary part), as would be expected for energies close to the Coulomb barrier. The adopted procedure describes remarkably well data for different systems in an extensive energy range, signaling that the main physics has been considered. In this sense, it offers a promising approach to analyze heavy-ion reactions well above the Coulomb barrier, when the couplings of the low-lying collective states can be strongly influenced by the couplings to very collective states in the continuum. Under these conditions, due to the large number of open channels and the possibility to access high excitation energies and multipolarities, the overall couplings can be accounted for in the calculations by deforming the imaginary part of nuclear potential.

An analysis of the resulting potentials was performed. They were composed by the Coulomb and nuclear interactions, added by the trivially equivalent local potential (TELP) [53] implemented in FRESCO code for each individual coupled channel. It is important to mention that one-channel calculations that includes the TELP have been proven to give a quite reasonable description of the CC elastic angular distribution, even in the case of a system involving weakly bound nuclei [54]. For the qualitative analysis here proposed, it is sufficient to use such an approximation. In Fig. 5, the effective potentials are presented for the real and imaginary parts. For the real part, the Coulomb potential is also included. Figures 5(a) and 5(b) show the real and imaginary parts (respectively) of the total potential for the $^{16}\text{O} + ^{60}\text{Ni}$ system. Figures 5(c) and 5(d) show the same potentials for the $^{16}\text{O} + ^{27}\text{Al}$ reaction (exclusively at 280 MeV).

An analysis of Figs. 5(a) and 5(c) shows that the effect of coupling the inelastic channels of the target and projectile (deforming the imaginary potential) affects the inner part of the barrier, especially changing the region close to the surface, defined, as usual, to be around the potential radius (indicated by the black arrows). The changes in the real part of the total potential accompany the changes (in the same region) of the imaginary part of the optical potential, as can be seen in Figs. 5(b) and 5(d). Both imaginary potentials became less absorptive, thus enhancing nuclear transparency in the overlapping region of the colliding nuclei. From Figs. 5(a) and 5(c), it is observed that the effect of the real DPP is to slightly widen the Coulomb barrier. Accordingly, considering the DPP is a one-effective-channel description, one can assert that such an added potential to the bare one induces a repulsive real and a weakening of the imaginary components. This is the opposite of what happens in the surface region at lower energies, or when one disregards the deformation of the imaginary part (check the red-dotted line in Fig. 5). This may indicate the necessity of including even the breakup channel since here the energy is quite high and such coupling may be relevant. Further work is required to elucidate the matter.

In general, it is not easy to guess the expected effect of the polarization potentials on the elastic and inelastic angular distributions. The real and imaginary parts may have different effects on the elastic and inelastic scattering depending whether they are attractive or repulsive. From Fig. 2(a), it is observed that coupling the inelastic channels of the target decreases the elastic differential cross sections of the $^{16}\text{O} + ^{60}\text{Ni}$ reaction at
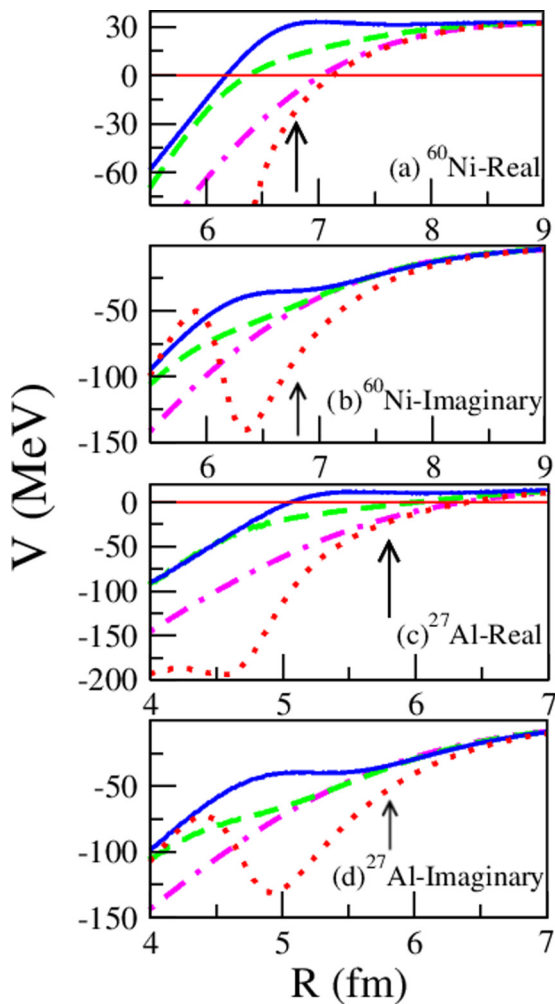
FIG. 5. Effective potentials. (a) Real polarization potential shape for several calculations of $^{16}O + ^{60}Ni$ reaction. (b) Imaginary polarization potential shape for several calculations of $^{16}O + ^{60}Ni$ reaction. (c) Imaginary polarization potential shape for several calculations of $^{16}O + ^{27}Al$ reaction. (d) Imaginary polarization potential shape for several calculations of $^{16}O + ^{27}Al$ reaction. The arrows represent the approximate potential radius position. The line type, color, and color code are the same as in Figs. 2 and 3.

backward angles. Then, coupling the inelastic channel of the projectile (blue solid line) affects especially the angular region between $\theta_{c.m.} = 30°$ and $\theta_{c.m.} = 45°$, increasing its differential cross section. For the $^{16}O + ^{27}Al$ system [Fig. 3(a)], the opposite occurs. As already mentioned, the net effect of the polarization potentials depends on the relative importance of the real and imaginary parts of total potential. For the $^{16}O + {}^{60}Ni$ case, the polarization potential acted close to the surface, affecting a small region of scattering angles. One should note

that to properly describe data, changes must occur only at particular values of the radius positions of the polarization potential. These local changes indicate that it is not possible, for instance, to simply find a normalization of the imaginary part that generates an effective potential which would describe the scattering in the the whole angular distribution. Figure 5 shows, for both systems, two aspects: (1) the necessity of using the deformation of the imaginary part of potential to generate an exclusively repulsive polarization potential and (2) the important role played by the projectile excitation, since the coupling to the 3^- state of ^{16}O is the one that produces more changes in the shape of the surface of the potential, being the responsible for the changes in the elastic scattering angular distributions. However, one must remember that both effects must be coupled to give a proper description of the angular distribution.

V. CONCLUSIONS

In summary, we have successfully described the elastic and inelastic scattering of $^{16}O + ^{60}Ni$ and $^{16}O + ^{27}Al$ at intermediate energies, through a coupled-channel calculation involving a deformed optical potential operator. We demonstrated that the deformed imaginary part of the potential, together with the inclusion of the excited 3^- state of ^{16}O, were important to get a good description of the data. In particular, the role played by the 3^- state of the ^{16}O projectile in the calculations was found to be of paramount importance. New perspectives are open to extend this exploration to other projectile-target systems and at other incident energies. In addition, an accurate investigation of the effect of coupling to the continuum, accessible with ^{16}O scattering at intermediate energy, can provide precious information on similar effects in weakly bound nuclei. In fact, in these latter systems, one expects a strong coupling to continuum even at energies around the Coulomb barrier. The precise description of heavy-ion elastic scattering can play a major role for a precise determination of nuclear matrix elements to be extracted from reaction studies. Pertinent examples are the recent studies of heavy-ion charge exchange reactions and their connection with neutrinoless double-β decay [24,55].

[1] M. A. Nagarajan, C. C. Mahaux, and G. R. Satchler, Phys. Rev. Lett. **54**, 1136 (1985).

[2] G. R. Satchler, Phys. Rep. **199**, 147 (1991).

[3] M. E. Brandan and G. R. Satchler, Phys. Rep. **285**, 143 (1997).

[4] M. S. Hussein, P. R. S. Gomes, J. Lubian, and L. C. Chamon, Phys. Rev. C **73**, 044610 (2006).

[5] C. Signorini, A. Andrighetto, M. Ruan, J. Y. Guo, L. Stroe, F. Soramel, K. E. G. Löbner, L. Müller, D. Pierroutsakou, M. Romoli, K. Rudolph *et al.*, Phys. Rev. C **61**, 061603(R) (2000).

[6] A. Pakou, N. Alamanos, G. Doukelis, A. Gillibert, G. Kalyva, M. Kokkoris, S. Kossionides, A. Lagoyannis, A. Musumarra, C. Papachristodoulou *et al.*, Phys. Rev. C **69**, 054602 (2004).

[7] S. B. Moraes, P. R. S. Gomes, J. Lubian, J. J. S. Alves, R. M. Anjos, M. M. S. Anna, I. Padron, C. Muri, R. L. Neto, and N. Added, Phys. Rev. C **61**, 064608 (2000).

[8] A. Kundu, S. Santra, A. Pal, D. Chattopadhyay, R. Tripathi, B. J. Roy, T. N. Nag, B. K. Nayak, A. Saxena, and S. Kailas, Phys. Rev. C **95**, 034615 (2017).

[9] V. A. B. Zagatto, J. Lubian, L. R. Gasques, M. A. G. Alvarez, L. C. Chamon, J. R. B. Oliveira, J. A. Alcántara-Núñez, N. H. Medina, V. Scarduelli, A. Freitas, I. Padron *et al.*, Phys. Rev. C **95**, 064614 (2017).

[10] V. Soukeras, A. Pakou, F. Cappuzzello, L. Acosta, C. Agodi, N. Alamanos, S. Calabrese, D. Carbone, M. Cavallaro, A. Cunsolo *et al.*, Phys. Rev. C **95**, 054614 (2017).

[11] A. Pakou, F. Cappuzzello, N. Keeley, L. Acosta, C. Agodi, X. Aslanoglou, S. Calabrese, D. Carbone, M. Cavallaro, A. Foti *et al.*, Phys. Rev. C **96**, 034615 (2017).

[12] D. A. Goldberg and S. M. Smith, Phys. Rev. Lett. **29**, 500 (1972).

[13] D. A. Goldberg, S. M. Smith, H. G. Pugh, P. G. Roos, and N. S. Wall, Phys. Rev. C **7**, 1938 (1973).

[14] D. A. Goldberg, S. M. Smith, and G. F. Burdzik, Phys. Rev. C **10**, 1362 (1974).

[15] D. T. Khoa, W. von Oertzen, H. G. Bohlen, and S. Ohkubo, J. Phys. G: Nucl. Part. Phys. **34**, R111 (2007).

[16] L. F. Canto, P. R. S. Gomes, R. Donangelo, and M. S. Hussein, Phys. Rep. **424**, 1 (2006).

[17] N. Keeley, R. Raabe, N. Alamanos, and J. L. Sida, Prog. Part. Nucl. Phys. **59**, 579 (2007).

[18] N. Keeley, N. Alamanos, K. W. Kemper, and K. Rusek, Prog. Part. Nucl. Phys. **63**, 396 (2009).

[19] B. B. Back, H. Esbensen, C. L. Jiang, and K. E. Rehm, Rev. Mod. Phys. **86**, 317 (2014).

[20] L. F. Canto, P. R. S. Gomes, R. Donangelo, J. Lubian, and M. S. Hussein, Phys. Rep. **596**, 1 (2015).

[21] K. Kisamori, S. Shimoura, H. Miya, S. Michimasa, S. Ota, M. Assie, H. Baba, T. Baba, D. Beaumel, and M. Dozono, Phys. Rev. Lett. **116**, 052501 (2016).

[22] D. Pereira, R. Linares, J. R. B. Oliveira, J. Lubian, L. C. Chamon, P. R. S. Gomes, A. Cunsolo, F. Cappuzzello, M. Cavallaro, D. Carbone, and A. Foti, Phys. Lett. B **710**, 426 (2012).

[23] F. Cappuzzello, D. Carbone, M. Cavallaro, M. Bondì, C. Agodi, F. Azaiez, A. Bonaccorso, A. Cunsolo, L. Fortunato, A. Foti *et al.*, Nat. Commun. **6**, 6743 (2016).

[24] F. Cappuzzello, M. Cavallaro, C. Agodi, M. Bondì, D. Carbone, A. Cunsolo, and A. Foti, Eur. Phys. J. A **51**, 145 (2015).

[25] S. Ohkubo and Y. Hirabayashi, Phys. Rev. C **89**, 051601(R) (2014).

[26] F. Cappuzzello, D. Nicolosi, R. Linares, J. R. B. Oliveira, J. Lubian, C. Agodi, D. Carbone, M. Cavallaro, P. N. de Faria, A. Foti, and M. R. D. Rodrigues, Eur. Phys. J. A **52**, 169 (2016).

[27] A. Cunsolo, F. Cappuzzello, M. Cavallaro, A. Foti, A. Khouaja, S. E. A. Orrigo, J. S. Winfield, L. Gasparini, G. Longo, T. Borello-Lewin *et al.*, Eur. Phys. J. A **150**, 343 (2007).

[28] F. Cappuzzello, C. Agodi, M. Cavallaro, and D. Carbone, Eur. Phys. J. A **52**, 6 (2016).

[29] M. Cavallaro, F. Cappuzzello, D. Carbone, A. Cunsolo, A. Foti, A. Khouaja, M. R. D. Rodrigues, J. S. Winfield, and M. Bondì, Eur. Phys. J. A, **48**, 59 (2012).

[30] F. Cappuzzello, D. Carbone, and M. Cavallaro, Nucl. Instrum. Methods A **638**, 74 (2011).

[31] M. Cavallaro, F. Cappuzzello, D. Carbone, A. Cunsolo, A. Foti, and R. Linares, Nucl. Instrum. Methods A **637**, 77 (2011).

[32] M. Cavallaro, F. Cappuzzello, D. Carbone, A. Cunsolo, A. Foti, R. Linares, D. Pereira, J. R. B. Oliveira, P. R. S. Gomes, J. Lubian, and R. Chen, Nucl. Instrum. Methods A **648**, 46 (2011).

[33] F. Cappuzzello, C. Agodi, M. Bondì, D. Carbone, M. Cavallaro, A. Cunsolo, M. De Napoli, A. Foti, D. Nicolosi, S. Tropea *et al.*, Nucl. Instrum. Methods A **763**, 314 (2014).

[34] D. H. Youngblood, Y. W. Lui, U. Garg, and R. J. Peterson, Phys. Rev. C **45**, 2172 (1992).

[35] See Supplemental Material at http://link.aps.org/supplemental/10.1103/PhysRevC.97.054608 for tables of the scattering data.

[36] I. J. Thompson, Comput. Phys. Rep. **7**, 167 (1988).

[37] M. A. Candido Ribeiro, L. C. Chamon, D. Pereira, M. S. Hussein, and D. Galetti, Phys. Rev. Lett. **78**, 3270 (1997).

[38] L. C. Chamon, D. Pereira, M. S. Hussein, M. A. Cândido Ribeiro, and D. Galetti, Phys. Rev. Lett. **79**, 5218 (1997).

[39] L. C. Chamon, B. V. Carlson, L. R. Gasques, D. Pereira, C. DeConti, M. A. G. Alvarez, M. S. Hussein, M. A. Candido Ribeiro, E. S. Rossi, and C. P. Silva, Phys. Rev. C **66**, 014610 (2002).

[40] M. A. G. Alvarez, L. C. Chamon, M. S. Hussein, D. Pereira, L. R. Gasques, E. S. Rossi, Jr., and C. P. Silva, Nucl. Phys. A **723**, 93 (2003).

[41] M. S. Hussein, R. A. Rego, and C. A. Bertulani, Phys. Rep. **201**, 279 (1991).

[42] G. R. Satchler, *Direct Nuclear Reactions* (Oxford University Press, New York, 1983), p. 616.

[43] K. Alder, A. Bohr, T. Huus, B. Mottelson, and A. Winther, Rev. Mod. Phys. **28**, 432 (1956).

[44] D. L. Hill and J. A. Wheeler, Phys. Rev. **89**, 1102 (1953).

[45] G. R. Satchler, Phys. Lett. B **33**, 385 (1970).

[46] I. Boztosun, M. Karakoc, and Y. Kucuk, Phys. Rev. C **77**, 064608 (2008).

[47] S. Raman, C. W. Nestor, and P. Tikkanen, At. Data Nucl. Data Tables **78**, 1 (2001).

[48] T. Kibédi and R. H. Spear, At. Data Nucl. Data Tables **80**, 35 (2002).

[49] L. C. Chamon and B. V. Carlson, Nucl. Phys. A **846**, 1 (2010).

[50] J. Suhonen, *From Nucleons to Nucleus: Concepts of Microscopic Nuclear Theory* (Springer, Berlin, 2007), p. 268.

[51] http://www.nndc.bnl.gov/ensdf/.

[52] A. Gomez-Camacho, E. Martinez-Quiroz, and T. Udagawa, Nucl. Phys. A **635**, 346 (1998).

[53] I. J. Thompson, M. A. Nagarajan, J. S. Lilley, and B. R. Fulton, Phys. Lett. B **157**, 250 (1985).

[54] J. Rangel, J. Lubian, L. F. Canto, and P. R. S. Gomes, Phys. Rev. C **93**, 054610 (2016).

[55] F. Cappuzzello, C. Agodi, M. Bondì, D. Carbone, M. Cavallaro, and A. Foti, J. Phys.: Conf. Ser. **630**, 012018 (2015).